# APPLICATION OF INDUSTRIAL ROBOT AND MACHINE VISION IN INTELLIGENT CALDRON FEEDING PROCESS OF CHINESE BAIJIU

/

# 工业机器人和机器视觉在中国白酒智能上甑工艺中的应用

**ZhongLing XIA[1,2], WeiHan CHEN[1)], Hang ZHAO[3)], WeiDong SONG*[4)], Ling YANG[1)], MingJin YANG*[1)]1)**

[1)]Southwest University, College of Engineering and Technology, Chongqing 400715, China

[2)]Chongqing Yottametre Industry Automation Co., Ltd., Chongqing 401122, China

[3)]Southwest University, College of Artificial Intelligence, Chongqing 400715, China

[4)]Ministry of Agriculture and Rural Affairs, Nanjing Institute of Agricultural Mechanization, Nanjing 210014, China

*Tel: +86 13883002509; E-mail: songwd@163.com; ymingjin@swu.edu.cn*

*DOI: https://doi.org/10.35633/inmateh-69-03*

***Keywords:*** *Chinese Baijiu, caldron feeding, industrial robot, machine vision, automatic distillation*

## ABSTRACT

*In traditional Chinese Baijiu (white wine) brewing factory, most processes were usually done manually. In order to promote industrial automation in liquor brewing industry and alleviate highly repetitive manual labor, an industrial robot operating system equipped with machine vision was designed to accomplish caldron feeding process during the distillation of Chinese Baijiu. Firstly, Modified D-H method was used to establish robot kinematics model. Shovel actuators and peripheral devices were designed to spread and transport grains during caldron feeding process. After that, an online detection system based on machine vision and master computer were designed to control key parameters of caldron feeding process, including grains height, caldron pressure, robot speed and waiting time, etc. Finally, multiple brewing experiments were carried out on crushed grains and spent grains. The experimental results showed that robot system maximum working space was 3.15 m, which could feed 3 caldrons at the same time. During Chinese Baijiu distillation, air pressure average error in caldron was 8.28 %. High proportion of first-class liquor and second-class liquor was obtained, which met engineering production requirements.*

## 摘要

*在中国传统的白酒酿造厂中，大部分工艺流程通常都是由人工完成。为了促进白酒酿造行业的工业自动化发展，减轻高重复性的人工劳作。本研究设计了一个配备机器视觉的工业机器人操作系统来完成中国白酒蒸馏过程中的上甑过程。首先采用改进的 D-H 方法对机器人进行数学建模，设计了铲式执行机构和外围设备用于上甑过程中大曲的铺料和运输。然后还开发了基于机器视觉的在线检测系统和上位机软件对上甑过程中的关键参数：料层高度，甑内压力，铺料速度和等待时间等进行控制。最后对大渣和丢糟两种原料进行多次酿造实验。实验结果表明：智能上甑机器人系统最大工作空间为 3.15m，可同时对 3 个甑桶进行上甑。白酒蒸馏过程中甑桶内气压平均误差为 8.28%。产出一级酒和二级酒的比例较高，符合工程生产要求。*

## INTRODUCTION

The six major distilled spirits in the world are brandy, whiskey, rum, vodka, gin and Chinese Baijiu (*Xie J. et al, 2022*). Chinese Baijiu uses solid-state fermentation and distillation process, which allows alcohol molecules in the fermented spirits to be distilled and purified. Through this process, flavor substances with special aromas are preserved intact (*Zhang G. Y. et al, 2017*). Caldron feeding process, as one of the core process steps in Chinese Baijiu brewing process, directly determines output rate and quality of liquor. In caldron feeding process, workers spread brewing ingredients in layers, evenly and loosely inside caldron to ensure that steam permeates upward from the bottom layer by layer to distill alcohol. Steam leakage or accumulation during spreading process will affect the quality of Chinese Baijiu (*Li Y., 2015*).

In traditional Chinese Baijiu brewing factory, caldron feeding process still required a lot of manual work (*Zhang J.S., 2017*). The process requires cooperation of two skilled operators, one of whom shovels ingredients from pile into dustpan, while the other spreads brewing ingredients from dustpan into 3m$^2$ caldron

---

*1) ZhongLing Xia, M.S. Eng.; WeiHan Chen, M.S. Stud. Eng.; Hang Zhao, M.S. Eng.; WeiDong Son,; Prof. Eng.; Ling Yang, Prof. Eng.; MingJin Yang, Prof. Eng.*

in layers. During the 35-40 min process, workers often have to repeat the shoveling and spreading action hundreds of times, and the total mass of brewing ingredients handled exceed 2000kg (*Yang Y. et al, 2021*). In addition, manual work was also accompanied by poor working conditions and inconsistent quality (*Qing Y. H., et al, 2020*). In recent years, industrial robots based on machine vision have been widely used to meet the automation and intelligence requirements of intelligent manufacturing. As the field of robotics continues to expand, it is possible for industrial robots to replace manual labor in caldron feeding process (*Jiang W.Y., 2022*). However, the caldron feeding machine on the market still suffers from poor accuracy in detecting the surface temperature of fermented grains, poor uniformity in spreading ingredients, and difficulty in controlling path planning and feeding time, etc. (*Li L.H. et al, 2018*).

In this paper, based on the traditional caldron feeding process and actual working requirements, an industrial robot operating system equipped with machine vision was designed, including robot arm, shovel actuator, machine vision system, master computer and control module, etc. According to layout of caldron and receiving port, the corresponding robot arm type and specification were selected. Modified D-H method was used to establish robot forward kinematics model. Then, applying Monte Carlo method to calculate robot working space to verify that the selected robot met caldron feeding requirements. An online detection system based on machine vision were designed to ensure quality of caldron feeding process. Finally, multiple brewing experiments were carried out on crushed grains and spent grains to verify feasibility of engineering application of intelligent robot caldron feeding system scheme.

## MATERIALS AND METHODS

### Mechanical system

#### *Robotic arm and shovel actuators*

The palletizing robot ABB IRB 660 was mainly composed of fixed base, rotary table, large arm, small arm, gripper mounting flange, joint drive motor, hydraulic cylinder and connecting rod. As shown in Fig. 1, IRB 660 with a 4-DOF parallelogram mechanism had 4 motors, driving rotary table rotation, large and small arms pitch, and gripper rotation, respectively. The working range of the four rotating parts was shown in Table 1. In addition, three links formed a double parallelogram mechanism, which was designed to always keep end-actuator parallel to the ground, so that palletizing robot gripped or placed objects smoothly. The stiffness to mass ratio of the robot was improved indirectly, then its weight and drive power were decreased.

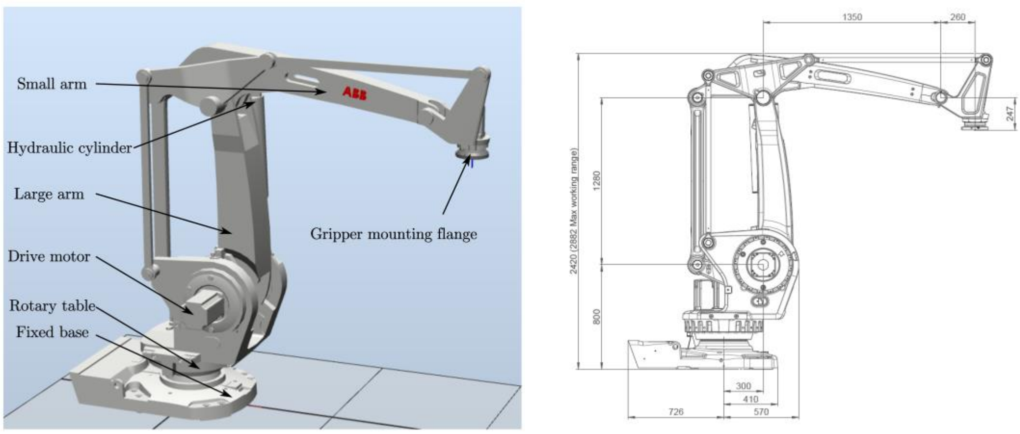


**Fig. 1 – IRB 660 model drawing**

**Table 1**

**IRB 660 Performance Parameters**

| Type: 660-180 | | Max. load: 180 kg | | Reach distance: 3.15 m | | Number of axes: 4 | |
|---|---|---|---|---|---|---|---|
| **Sport performance** | | | | | | | |
| **Axis 1** | | **Axis 2** | | **Axis 3** | | **Axis 4** | |
| Rotation range of $\beta_1$ [°] | Max. velocity [°/s] | Rotation range of $\beta_2$ [°] | Max. velocity [°/s] | Rotation range of $\beta_3$ [°] | Max. velocity [°/s] | Rotation range of $\beta_4$ [°] | Max. velocity [°/s] |
| -180 ~ 180 | 130 | -42 ~ 85 | 130 | -20 ~ 120 | 130 | -300 ~ 300 | 300 |

Shovel actuators were connected to robot arm by flanges. Fermented grains entered actuator at A, then they were transported by a conveyor belt at the bottom of actuator, and finally they spread by dispersing device at B. As shown in Fig. 2, the size of actuator was 475mm*600mm*400mm.

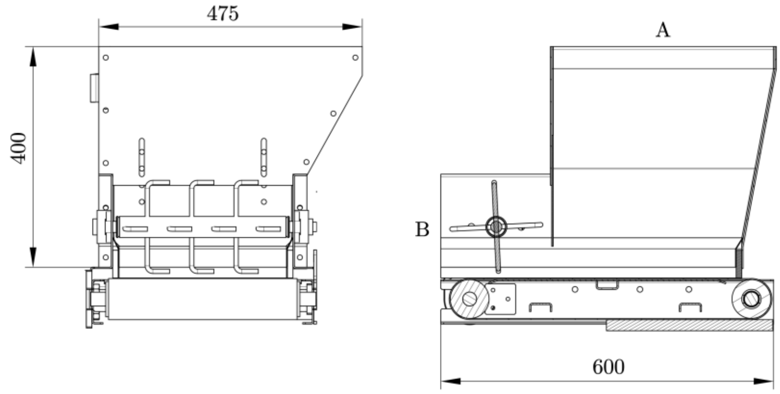


**Fig. 2 – Shovel actuator model**

***Peripheral Institutions***

Peripheral Institutions were equipped with cache hopper, fermented grains operating platform, closed cooler, auto-turning lid, auto-turning caldron, discharger and transfer conveyor. The 3-D diagram of system was shown in Fig. 3 (a), and physical diagram of system was shown in Fig. 3 (b).

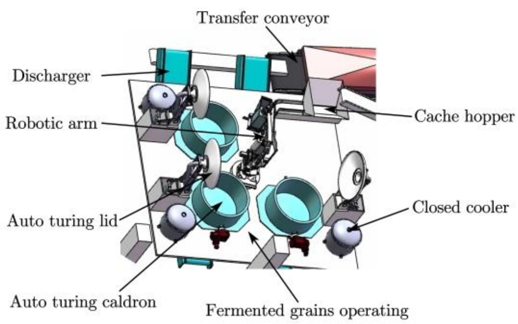


(a) 3-D diagram

(b) Physical diagram

**Fig. 3 – Caldron feeding system**

## Control system

***System device***

The control system mainly included IPC, robot controller, PLC (Siemens, S7-1200), demonstrator (ABB). Machine vision system included ultrasonic rangefinder, 3D camera and infrared thermal imager, etc. IPC was responsible for receiving data from others to coordinate entire workstation. S7-1200, as the main motion control device, interacted with the robot via the profinet protocol. Ultrasonic rangefinder feeds detected distance data back to IPC or PLC to adjust the height of caldron feeding process. Three caldrons shared a common machine vision system, and inspection device was fixed on stand, which could rotate above caldron respectively. The machine vision device and spatial layout of caldrons were shown in Fig. 4(a). The installation height of device was 4.5m. As shown in Fig. 4 (b), the outermost feeding radius of caldron $R_{f\max}$ was calculated by:

$$R_{\mathrm{f\,max}} = \frac{\sqrt{2}L_{\mathrm{c}} + D_{\mathrm{c}}}{2} \tag{1}$$

Where:

$R_{\mathrm{f\,max}}$ is max feeding radius, [mm]; $L_{\mathrm{c}}$ is the distance between caldron, [mm]; $D_{\mathrm{c}}$ is the inner diameter of caldron, [mm]. $R_{\mathrm{f\,max}}$ is 3.06 m.

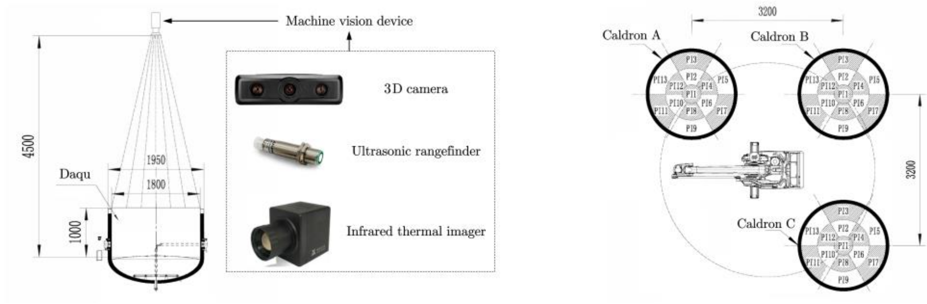


(a) Machine vision device and spatial layout of caldrons (b) Bird's view of caldrons

**Fig. 4 – Machine vision device and layout of caldrons**

### *Master host*

During caldron feeding process, master host controlled robot operating parameters. Main parameters included total height, layer height, current layer number, chain plate velocity, robot velocity and waiting time, etc. Auxiliary parameters included time for stopping feeding in advance and adjustment times. Minimum, maximum and stable air pressure in caldron could be adjusted by master host. In addition, master host monitored running status of robotic arm parameters, such as feeding cycle status, robot power status, shovel actuator coordinate position and manual operation interface. The cooperation of manual operation interface and teach pendant could replenish fermented grains at air leakage area after feeding. The flow chart of control system was shown in Fig. 5.

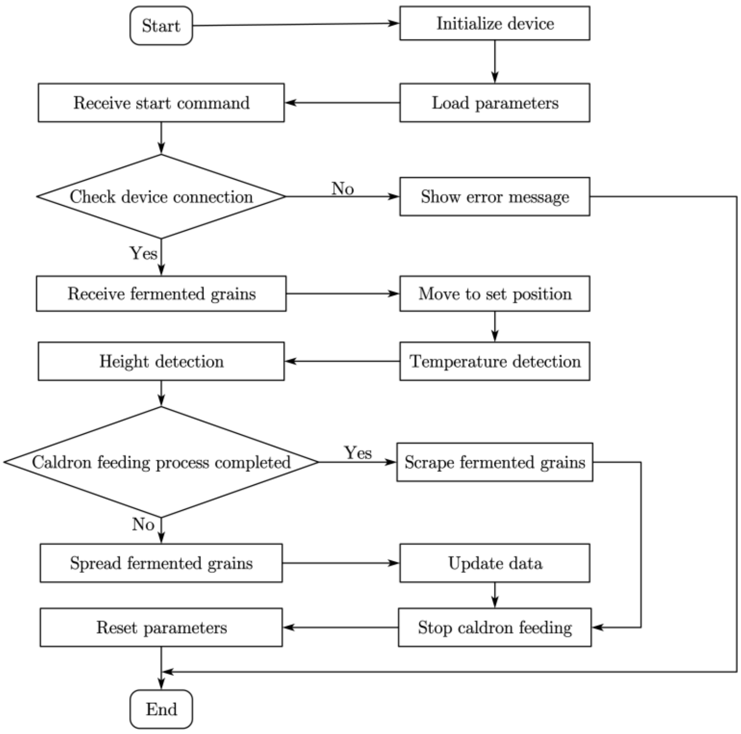


**Fig. 5 - Control system flow chat**

## RESULTS

### Motion model

According to above the analysis of palletizing robot IRB 660, a simplified structural diagram of robot was shown in Fig. 6 (a). $\theta_1$, $\theta_2$ and $\theta_3$ are rotation angles of rotary table, large arm and small arm respectively; $L_1$, $L_2$, $L_3$, $L_4$ and $L_5$ are lengths of waist, large arm, small arm, wrist and actuator link, respectively. Using modified D-H method to establish 4-DOF robot coordinate system, as shown in Fig. 6 (b), where $a_1$=300mm, $a_2$=1280mm, $a_3$=1350mm.

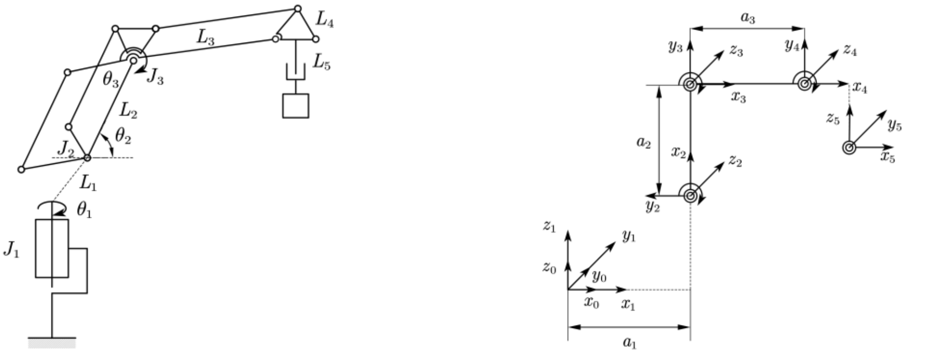


(a) Robot structure diagram (b) D-H coordinate system

**Fig. 6 - Robot structure diagram and D-H coordinate system**

Forward kinematics was applied to solve posture of actuator in Cartesian space through the value of movement or rotation of each joint of robot arm. According to Modified D-H method, a homogeneous transformation matrix ${}^{i\text{-}1}_{i}T$ was used to represent transformation from coordinate system *i*-1 to *i*. The ${}^{i\text{-}1}_{i}T$ was determined by (*Rong S. L. et al, 2010; Craig J. J. 2006*):

$$ {}^{i-1}_{i}T = \begin{bmatrix} c\theta_i & -s\theta_i & 0 & a_{i-1} \\ s\theta_i c\alpha_{i-1} & c\theta_i c\alpha_{i-1} & -s\alpha_{i-1} & -s\alpha_{i-1} d_i \\ s\theta_i s\alpha_{i-1} & c\theta_i s\alpha_{i-1} & c\alpha_{i-1} & c\alpha_{i-1} d_i \\ 0 & 0 & 0 & 1 \end{bmatrix} \tag{2} $$

where $c\theta_i = \cos(\theta_i)$, $s\theta_i = \sin(\theta_i)$, $c\alpha_i = \cos(\alpha_i)$, $s\alpha_i = \sin(\alpha_i)$.

According to Fig. 6 and Table 1, robot modified D-H parameters were listed in Table 2.

**Table 2**

**Modified D-H parameters**

| Joint i | $\alpha_{i\text{-}1}$ | $a_{i\text{-}1}$ | $d_i$ | $\theta_i$ | Range |
|---|---|---|---|---|---|
| 1 | 0 | 0 | 0 | $\theta_1$ | -180° ~ 180° |
| 2 | π/2 | $a_1$ | 0 | $\theta_2$ | -132 ~ -5 |
| 3 | 0 | $a_2$ | 0 | $\theta_3$ | 20° ~ 160° |
| 4 | 0 | $a_3$ | 0 | $\theta_4$ | $-\theta_2$ ~ $\theta_3$ |

When data in Table 2 were substituted into Eq. (2), the homogeneous transformation matrix between four coordinate systems were expressed as:

$$ {}^{0}T_1 = \begin{bmatrix} c\theta_1 & -s\theta_1 & 0 & 0 \\ s\theta_1 & c\theta_1 & 0 & 0 \\ 0 & 0 & 1 & 0 \\ 0 & 0 & 0 & 1 \end{bmatrix} \quad {}^{1}T_2 = \begin{bmatrix} c\theta_2 & -s\theta_2 & 0 & a_1 \\ 0 & 0 & -1 & 0 \\ s\theta_2 & c\theta_2 & 0 & 0 \\ 0 & 0 & 0 & 1 \end{bmatrix} $$
$$ {}^{2}T_3 = \begin{bmatrix} c\theta_3 & -s\theta_3 & 0 & a_2 \\ s\theta_3 & c\theta_3 & 0 & 0 \\ 0 & 0 & 1 & 0 \\ 0 & 0 & 0 & 1 \end{bmatrix} \quad {}^{2}T_3 = \begin{bmatrix} c\theta_4 & -s\theta_4 & 0 & a_3 \\ s\theta_4 & c\theta_4 & 0 & 0 \\ 0 & 0 & 1 & 0 \\ 0 & 0 & 0 & 1 \end{bmatrix} \tag{3} $$

The homogeneous transformation matrix of the end link relative to base coordinate system was defined as:

$$ {}^{0}T_4 = {}^{0}T_1 \, {}^{1}T_2 \, {}^{2}T_3 \, {}^{3}T_4 \tag{4} $$

$$ {}^{0}T_4 = \begin{bmatrix} c_1c_{234} & -c_1s_{234} & s_1 & c_1(a_1+a_3c_{23}+a_2c_2) \\ s_1c_{234} & -s_1s_{234} & -c_1 & s_1(a_1+a_3c_{23}+a_2c_2) \\ s_{234} & c_{234} & 0 & a_3s_{23}+a_2s_2 \\ 0 & 0 & 0 & 1 \end{bmatrix} \tag{5} $$

where $s_{234}=sin(\theta_1+\theta_2+\theta_3)$, $c_{234}=cos(\theta_1+\theta_2+\theta_3)$, $s_{23}=sin(\theta_2+\theta_3)$, $c_{23}=cos(\theta_2+\theta_3)$.

In addition, the positional relationship between shovel actuators and end link of robot was plotted in Fig.1. The posture matrix of shovel actuators was expressed as:

$$ {}^{0}T_5 = \begin{bmatrix} c_1c_{234} & -c_1s_{234} & s_1 & c_1(a_1+a_3c_{23}+a_2c_2)+260 \\ s_1c_{234} & -s_1s_{234} & -c_1 & s_1(a_1+a_3c_{23}+a_2c_2) \\ s_{234} & c_{234} & 0 & a_3s_{23}+a_2s_2-247 \\ 0 & 0 & 0 & 1 \end{bmatrix} \tag{6} $$

Meanwhile, the general representation of end link posture matrix was defined as (*Li J. L. et al, 2021*):

$$ T_5^0 = \begin{bmatrix} n_x & o_x & a_x & p_x \\ n_y & o_y & a_y & p_y \\ n_z & o_z & a_z & p_z \\ 0 & 0 & 0 & 1 \end{bmatrix} \tag{7} $$

Simultaneously solve Eq. (5) and Eq. (6), the forward kinematic equation was calculated by:

$$ \begin{cases} n_x = c_1c_{234} \\ n_y = s_1c_{234} \\ n_z = s_{234} \end{cases} \begin{cases} o_x = -c_1s_{234} \\ o_y = -s_1s_{234} \\ o_z = c_{234} \end{cases} \begin{cases} a_x = s_1 \\ a_y = -c_1 \\ a_z = 0 \end{cases} \begin{cases} p_x = c_1(a_1+a_3c_{23}+a_2c_2)+260 \\ p_y = s_1(a_1+a_3c_{23}+a_2c_2) \\ p_z = a_3s_{23}+a_2s_2-247 \end{cases} \tag{8} $$

When the motion conditions of each joint are known, posture of robot IRB 660 in base coordinate system can be calculated by Eq. (7).

**Workspace and static moment**

In order to express the working space of the robot visually, the Monte Carlo method in numerical method was used to calculated, and then MATLAB 2020b was used to draw a spatial point map to realize the visualization of working space of robotic arm. The detailed steps are as follows:

1. Forward kinematics equation was used to obatin transformation matrix of actuator in base coordinate system, where $P_x$, $P_y$, and $P_z$ represent position in space.

2. The random function Rand (j) in MATLAB was used to generate *N* numbers between 0 and 1 over each point motion range. The random values of each joint variable are represented as:

$$ \theta_i = \theta_{i\,\min} + (\theta_{i\,\max} - \theta_{i\,\min}) \times \mathrm{Rand}(j) \tag{9} $$

where $\theta_{i\,\min}$ and $\theta_{i\,\max}$ correspond to the minimum and maximum value of *i*-th joint variable, respectively.

3. Considering the influence of stop block and avoid mutual interference between members, there is a mutual constraint relationship between joint angles $\theta_2$ and $\theta_3$, as shown in Fig. 7 (a).

4. Marking the position of actuator in coordinate system to form three-dimensional point cloud image of the working space. The more random points there are, the closer to the actual working space of caldron feeding robot.

In this paper, the value of random point was set to 7000. The x-z plane and spatial result were displayed in Fig. 7 (b) and (c) respectively. There was no obvious hole in simulation, indicating that robot arm could move to various positions within working range. In the horizontal direction, the farthest distance that robot arm could reach was 3.15 m, which met the outermost caldron feeding radius 3.06 m. At the same time, in order to maximize production efficiency, three caldrons were arranged in working space to operate simultaneously.

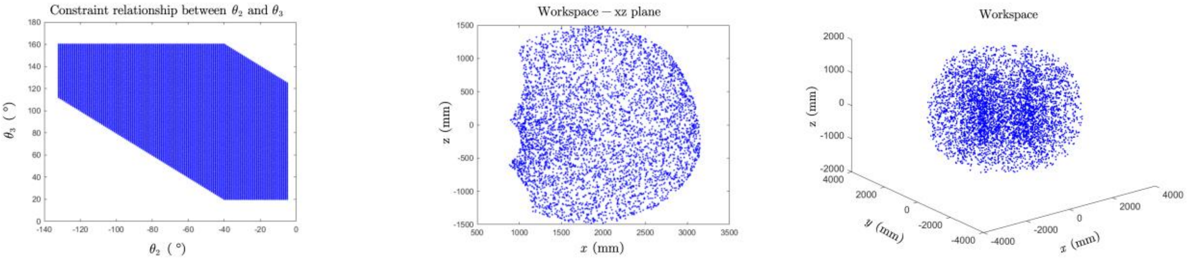

(a) Mutual constraint relationship between joint angles (b) Result of x-z plane (c) Spatial result

**Fig. 7 – Workspace of robot**

When the shovel actuator was fully loaded, maximum weight was 150 kg. Static moment analysis of the robot was obtained according to Fig. 6 (a):

$$\begin{aligned} &F_2 = F_3 = F = 1500\text{N} \\ &M_2 = F \times (L_2 \sin(-\beta_1) + L_3 \cos\beta_2 + 0.26) = 1500(1.35\cos\beta_2 - 1.28\sin\beta_1 + 0.26) \\ &M_3 = F \times (L_3 \cos\beta_2 + 0.26) = 1500(1.35\cos\beta_2 + 0.26) \end{aligned} \tag{10}$$

where $F$, $F_2$, $F_3$ are the forces on wrist, large arm and small arm respectively, [N]; $M_2$, $M_3$ are the hinge point moments of large arm and small arm respectively, [kNm].

As shown in Fig. 8, MATLAB was used to draw the state moment of hinge point. The maximum torque of large and small arm was 4.33 kNm and 2.42 kNm, respectively. The robot could operate safely within the preset range.

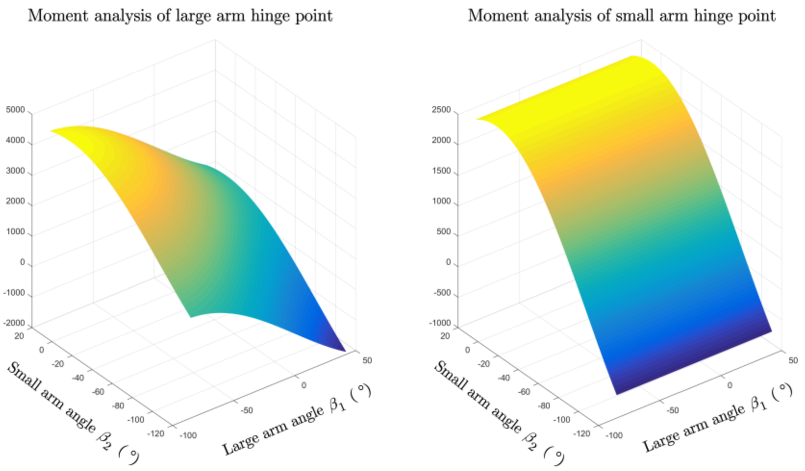

**Fig. 8 – Hinge Moment Analysis**

**Online detection system**

The online detection system of the intelligent caldron feeding system was divided into machine vision and air pressure monitoring system. The infrared thermal imager was used to monitor temperature of fermented grains surface inside the caldron in real time. When the surface occurred leaking gas, master host located position timely and accurately. Then the robot was controlled to feed fermented grains at leaking gas position. Simultaneously ultrasonic range finder and 3D camera worked together.

(a) Infrared image at start feeding (b) 3D image at start feeding (c) RGB image at start feeding

(d) Infrared image at midway feeding (e) 3D image at midway feeding (f) RGB image at midway feeding

**Fig. 9 – Online machine vision system**

As the height of the fermented grains increased, the area of lower temperature region photographed by infrared camera also increased. The fermented grains were spread evenly without air leakage on the surface, as shown in Figs. 9 (a) and (b). The increased blue area in Figs. 9 (b) and (e) taken by 3D camera also represented height increased. In addition, high resolution RGB photos of Figs. 9 (c) and (f) made it easy for operators to know feeding process of the caldrons.

Pressure monitoring system was shown in Table 2. Air pressure values in three caldrons were set in intelligent caldron feeding system and monitored every 10 minutes. According to Table 2, the average error of air pressure in caldron was 8.28 %, which met requirements of Chinese Baijiu production.

**Table 2**

**Air pressure monitoring value**

| Caldron number | Current pressure [bar] | State pressure [bar] | Max. pressure [bar] | Min. pressure [bar] | Set pressure [bar] | Error [%] |
|---|---|---|---|---|---|---|
| 1 | 2.2 | 2 | 2.2 | 1.7 | 2 | 10.00 |
| 1 | 2.05 | 2 | 2.2 | 1.7 | 2.2 | 6.82 |
| 1 | 1.98 | 1.8 | 2 | 1.7 | 1.8 | 10.00 |
| 2 | 1.97 | 1.7 | 2 | 1.6 | 2 | 1.50 |
| 2 | 1.84 | 1.7 | 1.8 | 1.5 | 1.8 | 2.22 |
| 2 | 1.8 | 1.7 | 1.8 | 1.5 | 1.7 | 5.88 |
| 3 | 1.17 | 1 | 1.2 | 0.9 | 1.2 | 2.50 |
| 3 | 1.07 | 0.8 | 1.1 | 0.7 | 0.8 | 33.75 |
| 3 | 1.12 | 0.8 | 1.1 | 0.7 | 1.1 | 1.82 |

**Production test**

The actual production application of the intelligent caldron feeding system was shown in Fig. 9. The states that fermented grains started to feed, feed in the midway and feed completed were shown in Fig. (a), (b) and (c) respectively.

(a) Feed starts (b) Midway of feeding (c) Feed complete

**Fig. 9 – Caldron feeding process**

Finally, the surface of fermented grains was paved, and caldron lid cover preparation was done for the distilling, and the distilling process lasted 1h approximately. Taking feeding process of caldron 1 as an example, the sets of some operating parameters in master host were shown in Table 3.

**Table 3**

**Sets of parameters of master host**

| Feed number | Inner-ring frequency [Hz] | Mid-ring frequency [Hz] | Outer-ring frequency [Hz] | Actual weight [kg] | Preset weight [kg] | Current height [mm] |
|---|---|---|---|---|---|---|
| 1 | 38 | 42 | 67 | 60.0 | 45 | 42 |
| 2 | 35 | 40 | 70 | 68.5 | 45 | 84 |
| 3 | 38 | 42 | 70 | 70.1 | 45 | 129 |
| 4 | 30 | 40 | 70 | 71.3 | 45 | 174 |
| 5 | 30 | 44 | 72 | 67.1 | 45 | 219 |
| 6 | 30 | 44 | 72 | 65.2 | 40 | 264 |
| 7 | 33 | 45 | 72 | 64.8 | 40 | 309 |
| 8 | 33 | 45 | 72 | 65.6 | 40 | 354 |
| 9 | 33 | 45 | 72 | 64.2 | 40 | 399 |
| 10 | 33 | 45 | 72 | 64.7 | 40 | 444 |
| 11 | 33 | 45 | 72 | 66.6 | 40 | 489 |
| 12 | 33 | 45 | 72 | 64.2 | 40 | 534 |
| 13 | 33 | 45 | 72 | 64.2 | 40 | 579 |
| 14 | 33 | 45 | 72 | 63.6 | 40 | 624 |
| 15 | 33 | 45 | 72 | 66.5 | 40 | 664 |
| 16 | 33 | 45 | 72 | 61.7 | 40 | 704 |
| 17 | 33 | 45 | 72 | 66.4 | 40 | 741 |
| 18 | 33 | 45 | 72 | 65.8 | 40 | 778 |
| 19 | 33 | 45 | 72 | 66.6 | 40 | 815 |
| 20 | 33 | 45 | 72 | 65.8 | 40 | 820 |
| 21 | 33 | 45 | 72 | 65.8 | 40 | 825 |
| 22 | 33 | 45 | 72 | 64.5 | 42 | 850 |
| 23 | 33 | 45 | 72 | 68.7 | 42 | 885 |
| 24 | 33 | 45 | 72 | 70.6 | 42 | 920 |

There were two raw materials in the actual distillation, namely crushed grains and spent grains, and they were distilled several times separately. The grade of Chinese Baijiu was analyzed. Figs. 10 (a), (b) and (c) represented liquor production curves of crushed grains. Figs. (d), (e) and (f) represented liquor production curves of spent grains. As distillation proceed, the temperature in caldron increased and reached 100°C eventually. The quality of Chinese Baijiu was mainly manifested in different compound aromas, and ethyl caproate was the main component. According to the *Chinese national standard GB/T10781.1-2021 (China National standardizing committee, 2021*), Chinese Baijiu was divided into first-class, second-class, and third-class liquor, respectively (*Wu W. Y. et al, 2022*). As shown in Fig. 10, 3 minutes after the distillation, temperature stabilized at around 85°C and caldron began to produce first-class or second-class Chinese Baijiu. When the temperature increased above 85°C, caldron started to produce third-class liquor. The total curve showed that output time ratio for first-class and second-class was much higher than for third-class, so the intelligent feeding system met the actual Chinese Baijiu production requirements.

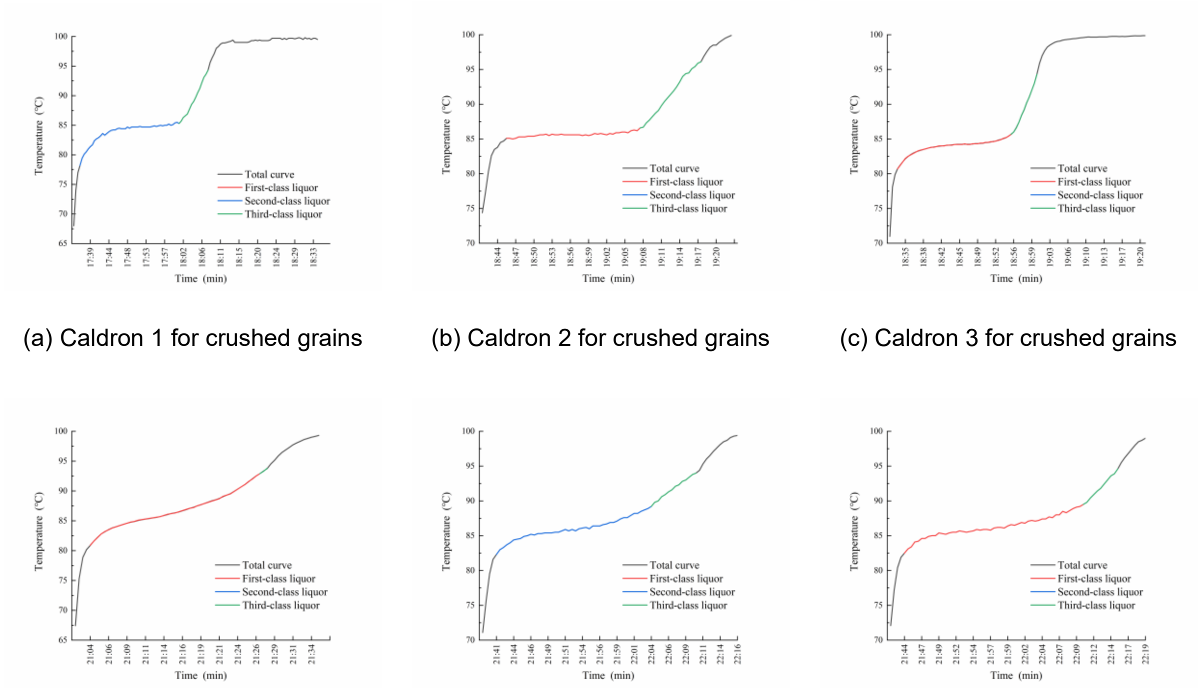


(a) Caldron 1 for crushed grains (b) Caldron 2 for crushed grains (c) Caldron 3 for crushed grains

(d) Caldron 1 for spent grains (e) Caldron 2 for spent grains (f) Caldron 3 for spent grains

**Fig. 10 – Chinese Baijiu brewing analysis**

## CONCLUSIONS

In this paper, an intelligent Chinese Baijiu caldron feeding system was designed, including industrial robot selection, machine vision system construction, shovel actuator and peripheral device design, etc. The actual brewing experiments of crushed grains and spent grains were carried out and analyzed. Main conclusions were drawn as follows:

(1) Modified D-H method was used to establish robot kinematics model. Monte Carlo method was used to analyze working space of robotic arm. The robot IRB 660 reached 3.15 m in horizontal direction, which was larger than the outermost caldron feeding radius 3.06 m. The maximum torque of large and small arm was 4.33 kNm and 2.42 kNm respectively. The robot IRB 660 met space and moment requirements of caldron feeding.

(2) An online detecting system with machine vision and air pressure monitoring was built. The caldron feeding process was displayed clearly in master host. There was no air leak on the surface of fermented grains in the feeding process. The air pressure monitoring result showed that air pressure inside caldron was stable, and average error between actual and set value was 8.28%.

(3) The crushed grains and spent grains were brewing in intelligent caldron feeding system. The first-class liquor and second-class liquor were produced around 85 °C, accounting for a high proportion of total curve, which met the actual requirements of Chinese Baijiu production and saved a lot of manual work cost.

## ACKNOWLEDGEMENTS

The study was funded by R & D Project of Chongqing Yottametre Industry Automation Co., Ltd. (No. ymdf20220909016).

## REFERENCES

[1] Craig J. J., (2006). *Introduction to Robotics*, Ed. Pearson Education, New York/USA;

[2] Jiang W. Y., (2022). *Design and Research of Upper-Retort-Robot Based on Machine Vision* (*基于机器视觉的探气上甑机器人设计与研究*). Master dissertation, Qilu University of Technology, Ji' nan/P. R. C.

[3] Li J. L., Zhang B., Shu H. R., Yang X. S., Liu A. J., (2021). Joint Velocity Planning of Loading and Unloading Robot (上下料机器人关节速度规划), *Science Technology and Engineering*, vol. 21, issue 14, pp. 5784-5788, Ed. China Association for Science and Technology, Beijing/P. R. C.;

[4] Li L. H., Wang R. W., Wen X. B., (2018). Design of Efficient Detection Algorithm for Spreading Area of Intelligent Steamer Feeding System Based on Infrared Vision (基于红外视觉的智能装甑系统的撒料区域的高效检测算法设计), *Journal of Tianjin University of Technology*, vol. 34, issue 6, pp. 49-53, Ed. Tianjin University of Technology, Tianjin/P. R. C.

[5] Li Y., Hua Y., (2015). Design of Mechanical Steaming Bucket Feeding Control System Based on PLC (机械装甄布料控制系统 PLC 设计), *Food & Machinery*, vol. 31, issue 4, pp. 70-73, Ed. Changsha University of Science & Technology, Changsha/P. R. C.

[6] Qing Y. H., Wang S. Q., Zhang Z. P., Zhou X. Y., (2020). Kinematics Analysis and Trajectory Research for Upper-Retort-Robot (上甑机器人运动学分析及轨迹研究), *Food & Machinery*, vol. 36, issue 12, pp. 70-73, Ed. Changsha University of Science & Technology, Changsha/P. R. C.

[7] Rong S.L., Yan H. L., (2010). Development of Universal Environment for Constructing 5-Axis Virtual Machine Tool Based on Modified D–H Notation and OpenGL. *Robotics and Computer Integrated Manufacturing*, vol. 26, issue 3, pp. 253-262. Ed. Elsevier Sci Ltd.

[8] Wu W. Y, Yuan L., Song W. J., Yang X. J., Su Z. Y., Zheng, R. X., Li, F. F., (2022). Changes of Physicochemical Requirements in the 2021 Edition of the National Standard for Nongxiang Baijiu (浓香型白酒国家标准 2021 版理化要求的变化分析), *Liquor-Making Science & Technology*, issue 6, pp. 17-25, Ed. Guizhou Provincial Light Industry Scientific Research Institute, Guizhou/ P. R. C.

[9] Xie J., Luo H. B., Zeng Y., Huang D., Huang Z. G., Wei C. H., Zhu L. L., (2022). Evolution and Research Status of Distillation Device in Chinese Baijiu Industry (中国白酒产业蒸馏装置的演变历程及研究现状), *China Brewing*, vol. 41, issue 2, pp. 9-14, Ed. Beijing Academy of Food Sciences, Beijing/P. R. C.

[10] Yang Y., Wang H. B., Zhang L. Y., Liu C., Sheng X. J., (2021). Robot Operation System for Caldron Feeding in Traditional Distillation of Chinese Liquor (面向上甑工艺的机器人作业系统研究), *Science Technology and Engineering*, vol. 21, issue 36, pp. 15516-15528, Ed. China Association for Science and Technology, Beijing/P. R. C.;

[11] Zhang G. Y., Tou X. G., Li S., Chen L., Tang K. Y., Peng Y. J., (2017). Application Status and Study on Steamer－Filling Robot in Traditional Distillation of Chinese Liquor (上甑机器人在白酒固态蒸馏中的应用现状与探讨), *Science and Technology of food Industry*, vol. 38, issue 13, pp. 216-219+224, Ed. Beijing Industrial Technology Research Institute, Beijing/P. R. C.

[12] Zhang J. S., (2017). *Design and Analysis of a New Feeding Robot* (*一种新型上甄机器人的设计和分析*). Master dissertation, Tianjin University of Technology, Tianjin/P. R. C.;

[13] *** China National standardizing committee, (2021), *Quality Requirements for Baijiu-Part 1: Nongxiangxing Baijiu, GB/T10781.1-2021* (*白酒质量要求第 1 部分：浓香型白酒, GB/T10781.1-2021*), Ed. Chinese Standard Press, Beijing/P. R. C.